



Numerical Calculation of Electrical Conductivity of Porous Electroceramics

CRISTIAN CIOBANU,¹ YUHUI LIU,² YUNZHI WANG² & BRUCE R. PATTON¹

¹*Department of Physics*

²*Department of Materials Science and Engineering, The Ohio State University, Columbus, OH, 43210*

Submitted July 15, 1998; Revised November 17, 1998; Accepted November 23, 1998

Abstract. A numerical method for the calculation of the electrical conductivity of porous ceramics for gas sensing applications is developed, which takes into account detailed microstructural features by mapping a mesoscopic irregular resistor network onto the microstructure. The overall conductance of the ceramic sample is obtained by solving the Kirchhoff equations for the irregular network using an efficient iterative algorithm. The method is designed to handle the widely varying conductivities of different microstructural components present in ceramic gas sensors. The evolution of the macroscopic conductance of the model systems during a phase field simulation of sintering is obtained and several characteristic stages are distinguished. The potential applications of the method in computer aided microstructural optimization for ceramic gas sensors is discussed.

Keywords: electrical conductivity, resistor network, microstructure, porous ceramics

1. Introduction

The transport properties of electroceramics depend critically on their microstructure which is characterized by the geometrical shapes, spatial arrangement and relative amount of microstructural components such as grains, pores, second phase particles and various interfacial boundaries. In many cases the design and manufacture of electroceramics for a particular application depends, to a large extent, on one's ability to tailor the microstructure through different processing techniques to achieve the desired properties. It is therefore essential to develop a quantitative way of characterizing the microstructure - property relationships in these materials.

The microstructures encountered in electroceramics such as oxide-based gas sensors are usually very complicated. Figure 1 shows a typical example of the microstructure observed in a TiO₂-based CO sensor. Since the electrical transport is very sensitive to the detailed microstructural features, simplifying assumptions for the geometry of the microstructure may result in significant deviations of the calculation

results from the actual values. For example, it has been shown that for the same microstructure, different effective medium models yield different estimates for the electrical conductance of the sample [2]. Therefore, reliable models capable of handling realistic microstructural features are essential for establishing a quantitative relationship between the microstructure and the electrical properties in electroceramics.

Over the past century, various analytical and numerical models have been developed to characterize the electrical conductivity of inhomogeneous media (see, e.g., [2] or [3] for recent reviews). However, the effect of pores, which are essential microstructural components of electroceramics used as gas sensors, has not been systematically investigated because of their complicated morphologies. In most of the literature, pores are either not considered or assumed to have very simple geometry and spatial distributions.

With the rapid advances in both processing speed and memory capacity of digital computers, numerical methods are now increasingly used in calculating the

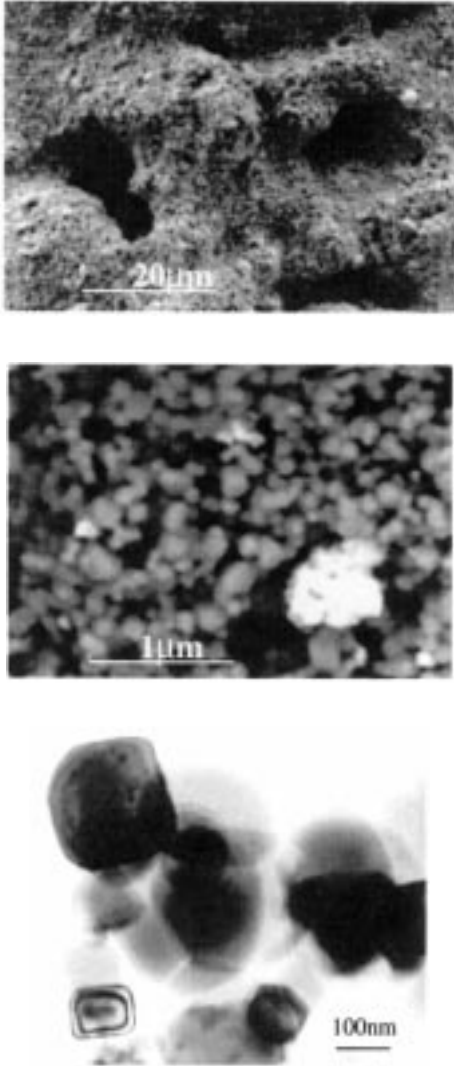


Fig. 1. Typical TEM image of a porous thin film microstructure used in a TiO_2 -based CO sensor ([1], courtesy of P. Gouma and M. Mills).

electrical properties of complex microstructures. These methods allow tackling a broad range of problems such as electrical conduction in polycrystalline materials [4], percolation in random mixtures of two components in which the conductivity of one component is much higher than that of the other [5,6], systems with exponentially distributed resistances [7] and systems with periodic microgeometry [8,9]. These methods have offered important insight into the microstructure-electrical property relationship for heterogeneous materials [2,4,8,9].

In this paper we study the microstructure—

electrical conductivity relationship in porous ceramic films which have three microstructural components (grain, grain boundary and pore) with very different conductivities. Typical thin film microstructures are simulated using the particle flow model [10] for the initial green compact and the continuum phase field model [11,12] for microstructural evolution. Since no geometrical constraints on the microstructures are imposed in this approach, finding the conductance of the porous ceramic film involves solving a three-value *arbitrary* resistor network problem which has not been discussed much in the literature. For example, only random three-component mixtures have been considered so far by the transfer-matrix method [2] and by the Monte-Carlo real space renormalization group method [13]. The microstructure of interest here (see, e.g., Fig. 1) is clearly not random and an accurate characterization of its electrical conductivity is essential in the design of ceramic gas sensors. In section 2 we describe the method in comparison with the standard relaxation-iteration algorithm [5]. In section 3 we apply this method to study the effect of various microstructural features of porous ceramic films on the conductivity of the material. An application illustrating the possibility of computational design of advanced microstructures for ceramic gas sensors is also described. Finally, our conclusions are presented in section 4.

2. Method

Description

For a given microstructure (obtained either from TEM/SEM measurements or from computer simulations) if the length scale of the conductive regions is large compared to the electronic mean free path, a local conductivity $\sigma(\mathbf{r})$ can be defined by the bulk value of conductivity of the material at point \mathbf{r} . Given $\sigma(\mathbf{r})$, one problem is to find the overall conductance G or, alternatively, the effective conductivity σ . A commonly used approach (e.g., [5,9]) for finding the effective conductivity of inhomogeneous media with a scalar local conductivity $\sigma(\mathbf{r})$ is to solve numerically the electrostatic equations $\nabla \cdot \mathbf{j} = 0$ and $\nabla \times \mathbf{E} = 0$, where the electric field \mathbf{E} and the current density \mathbf{j} obey the ohmic relation $\mathbf{j}(\mathbf{r}) = \sigma(\mathbf{r})\mathbf{E}(\mathbf{r})$.

It has long been recognized (see, e.g., [5]) that the finite difference solution to these equations is

formally equivalent to solving the Kirchoff's equations on a cubic (or square in two dimensions) resistor network superimposed onto the microstructure; the lattice constant has to be small enough to resolve the microstructural details. The conductance of the bond joining the nearest neighbor sites i and j of this network, g_{ij} , is proportional to the conductivity $\sigma(\mathbf{r})$ at the point \mathbf{r} between i and j [5].

The boundary condition for the problem is specified by applying an external potential difference $\Delta V = V_A - V_B$ to the ends of the network (Fig. 2). The current conservation condition for all bulk sites i reads:

$$\sum_j g_{ij}(V_i - V_j) = 0 \quad (1)$$

where V_i is the electrical potential at site i and the summation is taken over all nearest neighbors of site i .

There are various approaches for solving Eq. (1) such as the direct diagonalization method, the transfer matrix method [2,14], or the relaxation-iteration method [5]. In the present study we choose the relaxation-iteration method because the calculation time scales linearly with the system volume ($\mathcal{O}(N)$ algorithm). We first summarize how this method is used to solve a network with two values of the bond conductance (1 and α , with $\alpha < 1$) [5], and then discuss its application to a microstructure with pores, grains and grain boundaries.

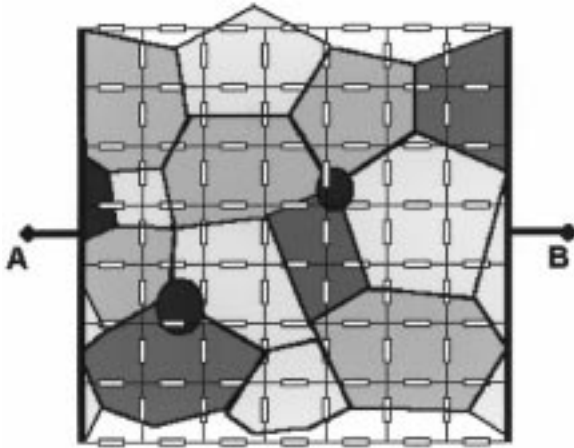


Fig. 2. Schematic drawing showing network discretization of a microstructure with equipotential boundary conditions on the left and right sides. The actual lattice constant of the resistor network used in calculations is much smaller than that shown here.

When $\alpha \sim 0.5$ one can start with a guess for the potentials $V_i^{(0)}$ and obtain the solution of Eq. (1) through direct iteration:

$$V_i^{(n+1)} = \frac{\sum_j g_{ij} V_j^{(n)}}{\sum_j g_{ij}} \quad (2)$$

where the superscript denotes the iteration index. However, when the ratio between the two values of the bond conductances is very small ($\alpha \ll 1$) direct iteration does not converge. In this case the solution to Eq. (1) may be obtained as the limit of a relaxation process. As the first step of this process one solves Eq. (2) for the network with the bond conductance ratio equal to 1/2 (typically). The solution is used as the initial guess in the next step in which the same network is solved with $\alpha = 1/4$. The process is continued until the desired value of α is reached.

This iterative procedure has been successfully used to study percolation as a critical phenomenon associated with resistor networks [5,6] and to test the validity of brick-layer models for conductivity calculations [4]. Two-phase composites consisting of regularly shaped and periodically distributed inclusions were recently studied; the dc conductivity, dielectric constant, and magnetoresistance were calculated using the iterative approach [9]. Irregular networks were studied in recent calculations [15] of electrical conductivity of two-phase composites consisting of fluid-saturated conducting pores and nonconducting circular particles.

The relaxation method has not been applied to microstructures with three components like that in Fig. 1, which would require two separate relaxation procedures. However, because the pore conductivity vanishes in our microstructure, the sites within the pores may be removed, reducing the problem to one with only two conductances. Although the network now contains under-coordinated sites (Fig. 3), the iteration procedure of Eq. (2) remains valid for this irregular network [5].

Implementation and Tests

The microstructures used in this study are obtained from the phase field simulation [11,12] (see [12] for a recent review of the phase field model). Microstructural development during sintering of a single phase material in the phase field model is described by the temporal evolution of a set of field

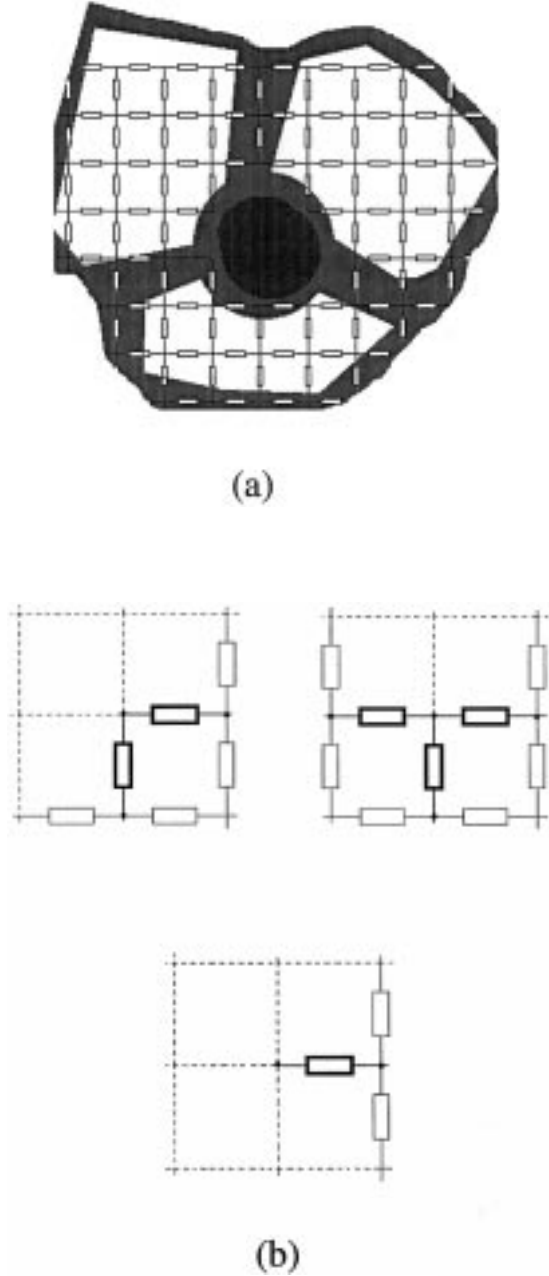


Fig. 3. (a) An example of an irregular resistor network associated with a 2D porous microstructure. (b) Possible environments of the sites belonging to an irregular network.

variables including the relative density field $\rho(\mathbf{r})$, which characterizes the density inhomogeneity of the system, and the long-range order (lro) parameter fields $\eta_p(\mathbf{r})$ ($p = 1, 2, \dots, n$) which characterize different crystallographic orientations of the grains [16]. The

time evolution of the density field during the sintering process is governed by the general non-linear diffusion equation:

$$\frac{\partial \rho(\mathbf{r}, t)}{\partial t} = \nabla \cdot \left[M \nabla \frac{\delta F}{\delta \rho(\mathbf{r}, t)} \right] \quad (3)$$

while the time evolution of the lro parameters are described by the time-dependent Ginzburg-Landau equation:

$$\frac{\partial \eta_p(\mathbf{r}, t)}{\partial t} = -L \frac{\delta F}{\delta \eta_p(\mathbf{r}, t)}, \quad (p = 1, 2, \dots, n) \quad (4)$$

In Eqs. (3) and (4) M and L are the kinetic coefficients characterizing diffusional and structural relaxations, n is the total number of lro parameters needed to characterize grain orientations, and F is the total free energy which is a functional of $\rho(\mathbf{r})$ and $\eta_p(\mathbf{r})$.

For a particular ceramic material the conductivity of the grain boundary (and possibly of the grain) may change during sintering due to impurity segregation at the interfaces. Although such effects may be included in our approach using the calculated or experimental data on the dependence of grain boundary conductivity on impurity concentration at grain boundaries, in the following we consider for simplicity the component conductivities to be fixed parameters throughout the sintering process. Since the grain boundary region in general is a region of increased scattering or activated barrier conduction, we model the local conductivity distribution $\sigma(\mathbf{r})$ as follows:

$$\sigma(\mathbf{r}) = \begin{cases} \sigma_g & \text{for } \mathbf{r} \text{ inside grain} \\ \sigma_{gb} = \alpha \sigma_g & \text{for } \mathbf{r} \text{ inside grain boundaries} \\ 0 & \text{for } \mathbf{r} \text{ inside pores} \end{cases} \quad (5)$$

where σ_g is the grain conductivity, σ_{gb} is the grain boundary conductivity and $\alpha = \sigma_{gb}/\sigma_g$ is a scaling factor (typically 0.01 to 0.001) whose value is determined by the relative conductivity of the grain boundary compared to the grain for the system considered. The bond conductance for two nearest neighbor sites is then given by $g_{ij} = \sqrt{\sigma_i \sigma_j}$ (for unit lattice constant).

To successfully implement the relaxation algorithm on the irregular network we employ neighbor tables [16]. For every site only the nearest neighbors with nonzero relative density are stored; similarly only the non-zero conductances of the bonds emerging from every individual site are stored. This

procedure ensures that the memory requirements of the method scale linearly with the number of sites in the microstructure.

A simple and straightforward way to test the model is to monitor the current conservation: the current flowing in through one end of the sample (A) has to be equal to the current emerging at the other end (B) (Fig. 2). Since a highly accurate equality requires large number of iterations, a difference of maximum 5% between the incoming and outgoing current is allowed. This brought the number of iterations in the range of 10,000s, an average task for today's workstations. The voltage applied to the finite sample is set to $\Delta V = 100$ so the error made in calculating the conductance G of the finite sample is less than 0.5%. Further tests also showed good convergence for the potentials at various sites inside the sample.

3. Results and Discussion

To investigate electrical property changes during sintering, the electrical conductivity of a finite sample during a phase field simulated sintering process Fig. 4(a) is calculated. Here we consider a two dimensional (2D) model system with thin film geometry. The initial green state of the sample is generated by the particle flow model [10], and consists of 100 particles of circular shapes with a 2D density of 65%.

Under the assumption discussed earlier that the ratio of the grain boundary conductivity to grain conductivity remains constant, the macroscopic conductivity σ of the sample (with current flowing from top to bottom in Fig. 4(a)) is calculated as the microstructure evolves during sintering. The results are shown in Fig. 4(b) for the case $\alpha = \sigma_{gb}/\sigma_g = 1/128$. For this initial density, the evolution of the overall conductivity σ vs. sintering time shows several distinct regions. First, there is a sharp increase in the conductivity as sintering starts caused by the formation of necks between particles. Initially, the interparticle contacts in the green state are poor and highly resistive, resulting in limited electrical conducting paths from one end of the sample to the other. As the sintering proceeds, necks between contacting particles start to develop, forming better conductive paths, leading to a sharp increase in the conductance of the sample. The microstructural evolution at this stage is characterized by shape

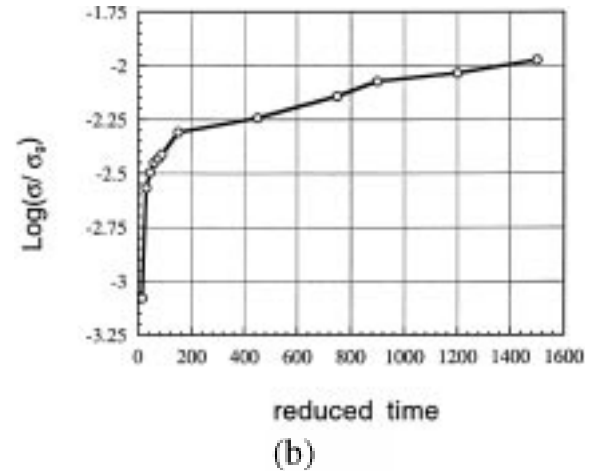
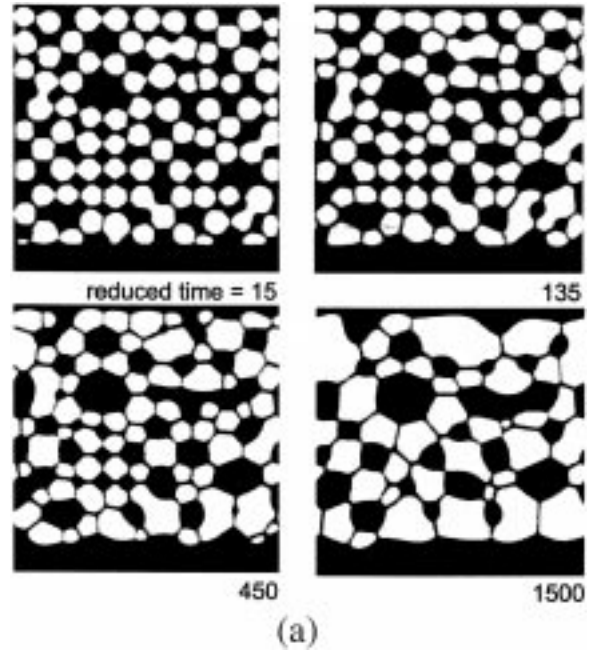


Fig. 4. (a) Microstructural evolution simulated by the phase field method for a 2D green compact of 65% relative density. (b) Change of the normalized electrical conductivity σ/σ_g of the sample during sintering. The grain boundary to grain conductivity ratio is $\sigma_{gb}/\sigma_g = 1/128$.

rearrangement in which pores change their shapes from concave to convex and grains change from convex to concave. After the neck formation, grains start to grow and pores are gradually eliminated from the sample. These processes reduce the fractions of the microstructural components of high resistance (e.g., pores and grain boundaries) in the sample, leading to a slower conductance drop with sintering

time compared to the rate of decrease in the early stages.

Since gas sensing is dominated by surface phenomena, it is desirable to have a high surface-to-volume ratio in the microstructure [18,19]. However, the above simulation results have shown that the microstructure developed at very early stages of sintering may not be suitable for sensor applications even though it has a high surface-to-volume ratios. This is because further sintering can take place when the material is in service, particularly when used in harsh environments. In this case both sintering and gas adsorption are responsible for resistance changes, which makes the measurements unreliable. For this reason the microstructure developed at the intermediate stage (see e.g. reduced time = 200~400 in Fig. 4(b)) is preferable because it optimizes both the sensitivity and stability of the material.

As seen in Fig. 1, the particles in a sensor film may be heavily agglomerated. In this case there are two distinct characteristic length scales: one associated with the microstructural features inside the agglomerates and the other associated with the size and spatial arrangement of the agglomerates. Each agglomerate contains grains, grain boundaries and pores. The effective conductivity σ_{eff} of an agglomerate can be calculated via the irregular network approach discussed above. At the level of the agglomerates, the microstructural components are pores with $\sigma_{pore} = 0$ and agglomerates with the conductivity $\sigma_{aggl} = \sigma_{eff}$. Such a two-valued resistor network problem is entirely tractable by the standard relaxation-iteration method [5]. However, the irregular network method is about 5 to 8 times faster than the standard approach because in this case there is only *one* component (the pores are discarded) with the bond conductance given by σ_{eff} . No relaxation is then necessary.

To investigate possible effects of particle agglomeration on the conductance of the sample in comparison with the effect of microstructural features inside the agglomerates, we studied various samples with different agglomerate structure. In particular, we considered structures with good contact (Fig. 1) as well as structures with weakly conducting necks between agglomerates. When the volume fraction of the agglomerate particles is reasonably high—about 5 to 10% higher than the percolation threshold of 50%—and the random agglomerates have good mutual contact, then the influence of the agglomerate

structure is essentially determined by the fraction of conducting material inside the agglomerate. This is in agreement with bond-percolation studies (e.g., [5]). In this case the microstructural features inside agglomerates determine the overall conductivity of the sample. However, if the agglomerates are poorly connected, the influence of the agglomerate structure could be strong.

To predict the performance of the samples as gas sensors, we need to characterize how their conductivity changes when they are exposed to ambient gases. This relationship may be obtained by comparison with experiments or simulation results on the grain and grain boundary conductivity change vs. reducing gas concentration [18,19]. When the sample is exposed to a certain gas, the conductivity of the grain boundary drops significantly (as shown, e.g., in [20]). The bulk conductivity of the grains also changes but to a much lesser extent [20,21]. Given the variation of the conductivity of these microstructural components as functions of the gas concentration, the sensing behavior of a given microstructure may be determined.

The relaxation method for the irregular network discussed above readily offers the capability to calculate the overall conductivity of the sample as a function the conductivity ratio between grain and grain boundary, σ_{gb}/σ_g . A typical example is given in Fig. 5, where the overall conductivity of a phase field simulated thin film is plotted as a function of σ_{gb}/σ_g . The results are in good qualitative agreement with the observed experimental trends for ceramic thin films [20].

4. Conclusion

To provide a way of directly correlating the detailed microstructural features developing during processing of ceramic gas sensors to their electrical conducting behavior, an irregular resistor network method has been developed which is able to characterize complex microstructures with very different component conductivities. The two dimensional simulation results have shown that combination of this method with microstructural modeling can provide a convenient tool for computer aided microstructural optimization of ceramic gas sensors. Systematic study of the effect of agglomeration, porosity, particle sizes, size distributions, and spatial arrangements on the sensing

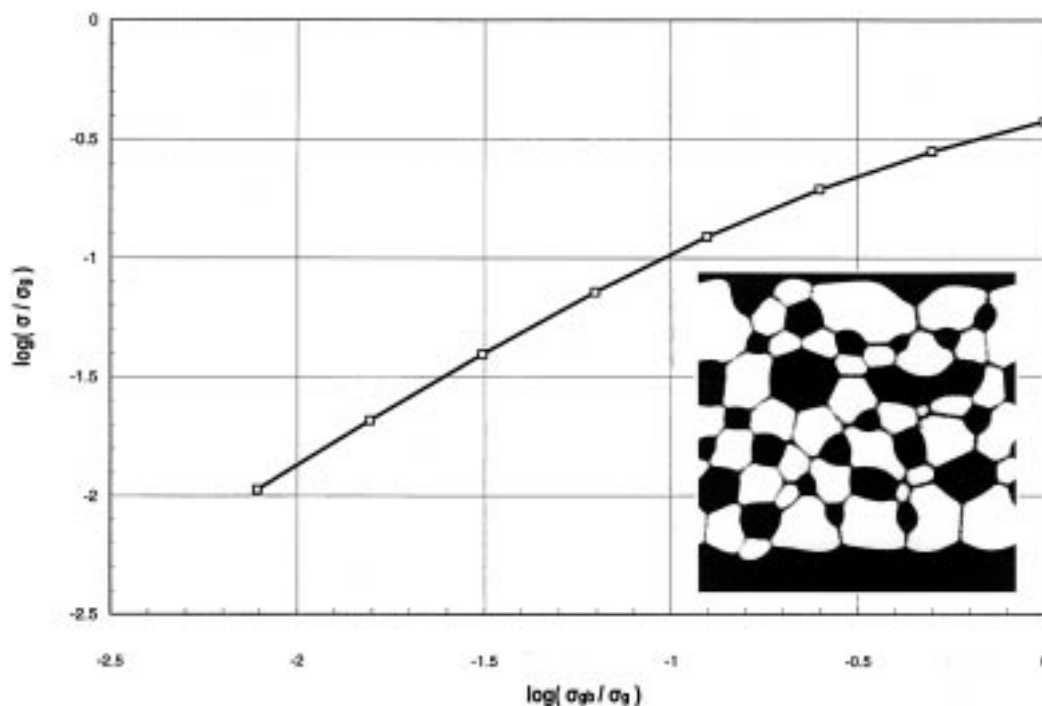


Fig. 5. The macroscopic conductivity σ of an phase field simulated microstructure vs. grain boundary conductivity σ_{gb} . Both conductivities are normalized by the grain conductivity σ_g .

behavior of ceramic gas sensors will be presented in a separate paper to follow.

Acknowledgment

It is a pleasure to acknowledge useful discussions with S. Akbar, P.K. Dutta, A. Ginwalla, P. Gouma, and M. Mills. This work was supported by National Science Foundation under Grant DMR 9703044 and the National Science Foundation Center for Industrial Sensors and Measurements under EEC-9523358 and DMR-9503429.

References

1. P. Gouma and M. Mills, in *Electron Microscopy and Analysis Group Conference (EMAG97) Proceedings*, (IOP Publishing Group, Ltd. 1997) p. 491.
2. D.G. Han and G.M. Choi, *Solid State Ionics*, **106**, 71 (1998).
3. J.R. Macdonald, *Impedance Spectroscopy*, (Wiley 1987), p. 193.
4. M.P. Anderson and S. Ling, *J. of Electronic Materials*, **19**, 1161 (1990).
5. S. Kirkpatrick, *Rev. Mod. Phys.*, **45**, 574 (1973).
6. J.P. Straley, *Phys. Rev. B*, **15**, 5733 (1977).
7. E.M. Baskin, A.A. Snarskii, A. Morozovskiy, J. Malinsky, and N. Abdellatif, *Phys. Rev. B*, **56**, 11611 (1997).
8. D.J. Bergman and K. Dunn, *Phys. Rev. B*, **45**, 13262 (1992).
9. K. Fisher and D. Stroud, *Phys. Rev. B*, **56**, 14366 (1997).
10. ITASCA Consulting Group Inc., *Particle Flow Code, Version 1.1, Users Manual* (1995).
11. Y. Liu, C. Ciobanu, Y. Wang, and B.R. Patton, preprint.
12. L.Q. Chen and Y. Wang, *JOM*, **48**, 13 (1996).
13. A. Koleck and A. Kusy, *Phys. Rev. B*, **43**, 11274 (1991).
14. B. Derrida and J. Vanniemenus, *J. Phys. A: Math. Gen.*, **15**, L557 (1982).
15. N. Martys and E.J. Garboczi, *Phys. Rev. B*, **46**, 6080 (1992).
16. L.Q. Chen, *Scripta Metall. Mater.*, **32**, 115 (1995).
17. M.P. Allen and D.J. Tildesley, *Computer Simulation of Liquids* (Oxford University Press 1987) p. 146.
18. P.K. Dutta, A. Ginwalla, B. Hogg, B.R. Patton, B. Chwierothe, Z. Liang, P. Gouma, M. Mills, and S. Akbar, preprint.
19. B.S. Chwierothe, B.R. Patton, and Y. Wang, preprint.
20. S.A. Akbar, L.B. Younkman, and P.K. Dutta, *Proceedings of the American Chemical Society Meeting* (Orlando 1996).
21. Ph. Odier, J.F. Baumard, D. Panis, and A.M. Anthony, *J. of Solid State Chem.*, **12**, 324 (1975).